JOURNAL OF MATERIALS SCIENCE 16 (1981) 3131–3140

Fracture properties of X-phase precipitation hardened ferritic stainless steel and ductility improvement of the steel

KATSUAKI SUGANUMA, HIDEO KAYANO, SEISHI YAJIMA
*The Oarai Branch, The Research Institute for Iron, Steel and Other Metals,
Tohoku University, Oarai, Ibaraki, 311-13 Japan*

The mechanical properties of Fe–13 wt% Cr–2 wt% Mo–2.5 wt% Ti alloy were examined by tensile tests with respect to its fracture mechanism. In order to improve the properties, 1 wt% Nb was added and its effects were examined. In the temperature range, room temperature to 500° C, the fracture characteristics of the alloys are mainly governed by the characteristics of the χ-phase precipitation. Fracture elongation is a function of $(C/r)^{1/2}$ where C is the radius of the χ-phase and r is its mean spacing. 1 wt% Nb addition is an effective method for improving the ductility without a decrease in the strength of the alloy.

1. Introduction

Ferritic stainless steels are known to have a good resistance to void-swelling [1–3] and helium embrittlement [4, 5] under severe fast neutron irradiation in fast breeder and controlled thermonuclear reactors. Up to now, several ferritic stainless steels have been developed [5–7]. The most important thing in developing new ferritic stainless steels is high temperature tensile strength and/or high temperature creep strength.

Recently, Huet and Leroy [5] developed a χ-phase strengthened ferritic alloy with a rupture strength comparable to that of type 316 austenitic stainless steel at 700° C [5, 7]. This ferritic alloy has the composition Fe–13 wt% Cr–(1.5 ~ 2) wt% Mo–(2.5 ~ 3.5) wt% Ti with or without the addition of 2 wt% TiO_2 or 1 wt% Y_2O_3. The excellent high temperature stress–rupture properties of the quaternary alloy are attributed to the formation of chi- (or χ)-phase precipitates along textures induced by cold-working.

In this research, we examined the relationship between the microstructures and the mechanical properties of this alloy and the effects of Nb addition as an alloying element.

2. Experimental procedure

The basic composition of the material was Fe–13 wt% Cr–2 wt% Mo–2.5 wt% Ti (Alloy 1). The amount of Nb addition was 1 wt% (Alloy 2). These alloys were prepared by arc melting in an argon atmosphere. Their chemical compositions are listed in Table I. The ingots were forged and rolled to 2 mm thickness at about 800 to 1000° C, and cold-rolled to 0.3 mm thickness sheets. Tensile specimens were cut from the sheets. They were aged at 800° C for 8 h and were air-cooled.

Microstructures were observed using a transmission electron microscope (JEM-200A), a scanning electron microscope and an optical microscope. The thin foils for electron microscopy were prepared with a double-jet electropolisher in a solution of 10% perchloric acid in acetic acid. Samples for optical microscopy were polished mechanically and this was followed by a chemical etch with 75% HF–75%HF–25%HNO_3 solution.

Tensile properties in the temperature range, room temperature to 600° C were investigated with an Instron-type tensile machine in vacuum. A strain rate of 1.96×10^{-4} sec^{-1} was chosen.

TABLE I Chemical composition (wt%)

Alloy	Cr	Mo	Ti	C	Nb	
1	12.8	2.23	2.33	0.007	–	balance Fe
2	13.0	2.14	2.30	0.010	0.97	

0022–2461/81/113131–10$03.00/0

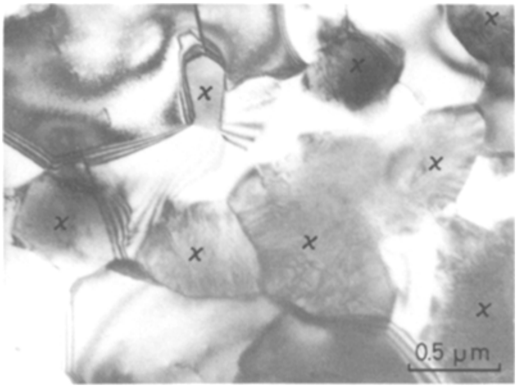

Figure 1 Microstructure of Alloy 1. Each χ-phase is marked as "χ".

3. Results

3.1. Microstructures

Fig. 1 shows the microstructure of Alloy 1. Each χ-phase, which is marked as "χ", exists as one grain and its diameter is about 1.0 μm which is comparable to the matrix grain size. The matrix is α-phase only and no sign of martensitic transformation is observed.

Fig. 2 shows the effects of Nb addition on χ-phase precipitation. In Alloy 1 the χ-phase precipitates are of diameter about 1.0 μm, of mean spacing about 1.0 μm and of volume fraction up to about 51% using a point counting method. On the other hand, in Alloy 2, two kinds of χ-phase precipitation appeared. One has a mean diameter of 2.5 μm and a mean spacing of about 3.5 μm. The other is very fine χ-phase precipitation with a diameter less than 0.5 μm and with a very dense distribution. The volume fraction of χ-phase precipitates of diameter larger than 0.1 μm is up to about 20%.

3.2. Tensile properties

Fig. 3 shows stress–strain curves of the two alloys at room temperature, 470° C and 600° C, respectively. Lüders deformation is recognized only in Alloy 2 in the temperature range, room temperature to 500° C. In this temperature range Alloy 1 shows a typical dispersion hardened ferritic alloy. Alloy 2 shows serration in the temperature range 250 to 500° C. Alloy 1 also sometimes shows rough serration, but this is not usual. At 600° C the differences in stress–strain curves between the two alloys is not clear.

Fig. 4 shows the tensile properties of two alloys as a function of temperature. Their 0.2% yield strengths show similar values in the whole temperature range. Ultimate tensile strengths are also similar to room temperature and 600° C but that of Alloy 2 is slightly lower than that of Alloy 1 in the serration temperature range. Total elongations show an apparent difference between the two alloys; that of Alloy 2 is larger than that of Alloy 1 in the whole temperature range, especially at room temperature when it is twice as large.

3.3. Fractography

Figs 5 and 6 show fracture surfaces tested at three temperatures. In Alloy 1, Fig. 5, although a fracture surface tested at room temperature shows an

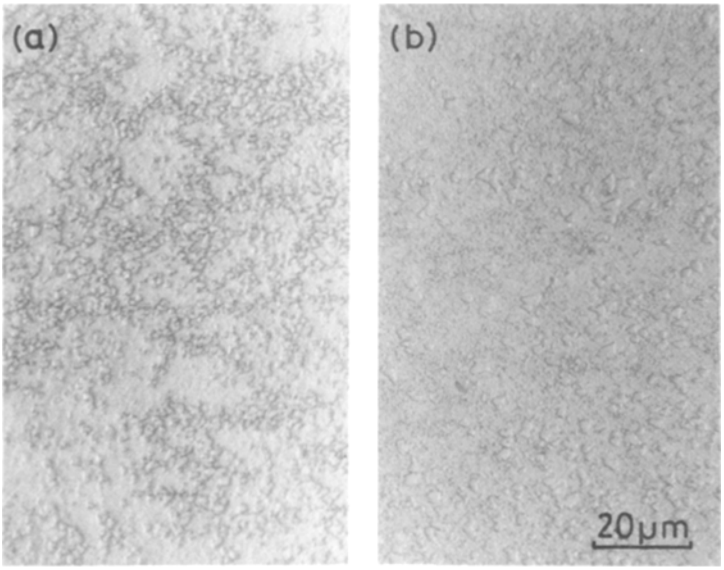

Figure 2 χ-phase precipitation change due to Nb addition: (a) Alloy 1 at room temperature and (b) Alloy 2 at 600° C.

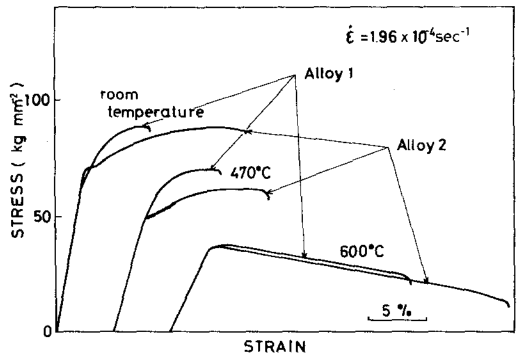

Figure 3 Stress–strain curve changes due to Nb addition at various temperatures.

appearance of brittle fracture macroscopically, it consists of fine dimples. The dimple diameter is about 1.0 μm. Faceted particles are usually observed in the bottom of the dimples. A fracture surface tested at 470° C shows large dimples in addition to fine dimples. On the fracture surface tested at 600° C, there is no fine dimple nor faceted particle.

In Alloy 2, Fig. 6, the fracture surface consists of two kinds of dimples at room temperature. One is larger than 1.0 μm in diameter and the other is about 0.5 μm in diameter. In large dimples faceted particles are usually observed.

Figs 7 and 8 show the distributions of cracks and slip steps on the free surface of deformed specimens. Fig. 7 shows the free surface of Alloy 1 at the onset of inhomogeneous deformation (just before fracture). When the inhomogeneous deformation begins, a deformation band, about 500 μm width, immediately crosses the specimen perpendicular to the stress axis. Many χ-phase crackings and slip steps are observed on the deformation band, but at a distance from it. χ-phase cracking occurs when a χ-phase meets a slip step. The number of χ-phase cracks on the longitudinal section of the specimen is far less than that on the free surface. Cracks occur at larger χ-phase ($\geqq$ 1.0 μm) easily and propagates to surrounding χ-phases in the direction perpendicular to the stress axis. Fig. 8 shows the free surface of Alloy 2 at the beginning of inhomogeneous deformation. In this alloy, there is no sign of the deformation band across the specimen but a deformation area which doesn't immediately cross the specimen. χ-phase cracking and slip steps are concentrated in this area. This is different from the case of Alloy 1 in which χ-phase cracking and slip steps are also observed far from the deformation area. On the longitudinal section of the specimen, there is no sign of the propagation of χ-phase cracking in the direction perpendicular to the stress axis but void-growth occurs in the direction parallel to the stress axis at the cracked χ-phases. No cracking of small χ-phase ($\leqq$ 0.5 μm) is observed.

Free surfaces of Alloy 1 and Alloy 2 tested at 600° C show no χ-phase cracking but separation of the interface between the χ-phase and the matrix.

4. Discussion

4.1. Fracture mechanism of Fe–13 wt % Cr–2 wt % Mo–2.5 wt % Ti alloy in the temperature range, room temperature to 500° C

In this alloy, little χ-phase was observed far from the deformation band. This indicates that χ-phase cracking starts at the beginning of inhomogeneous deformation and before that the alloy can take a strain of about 6%.

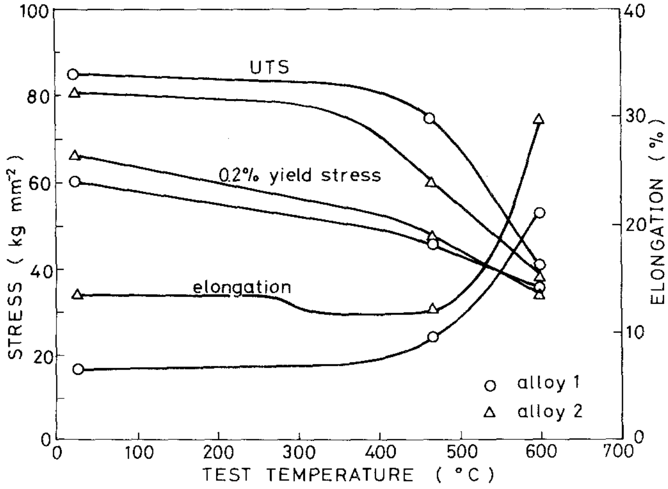

Figure 4 Tensile properties changes due to Nb addition as a function of test temperature.

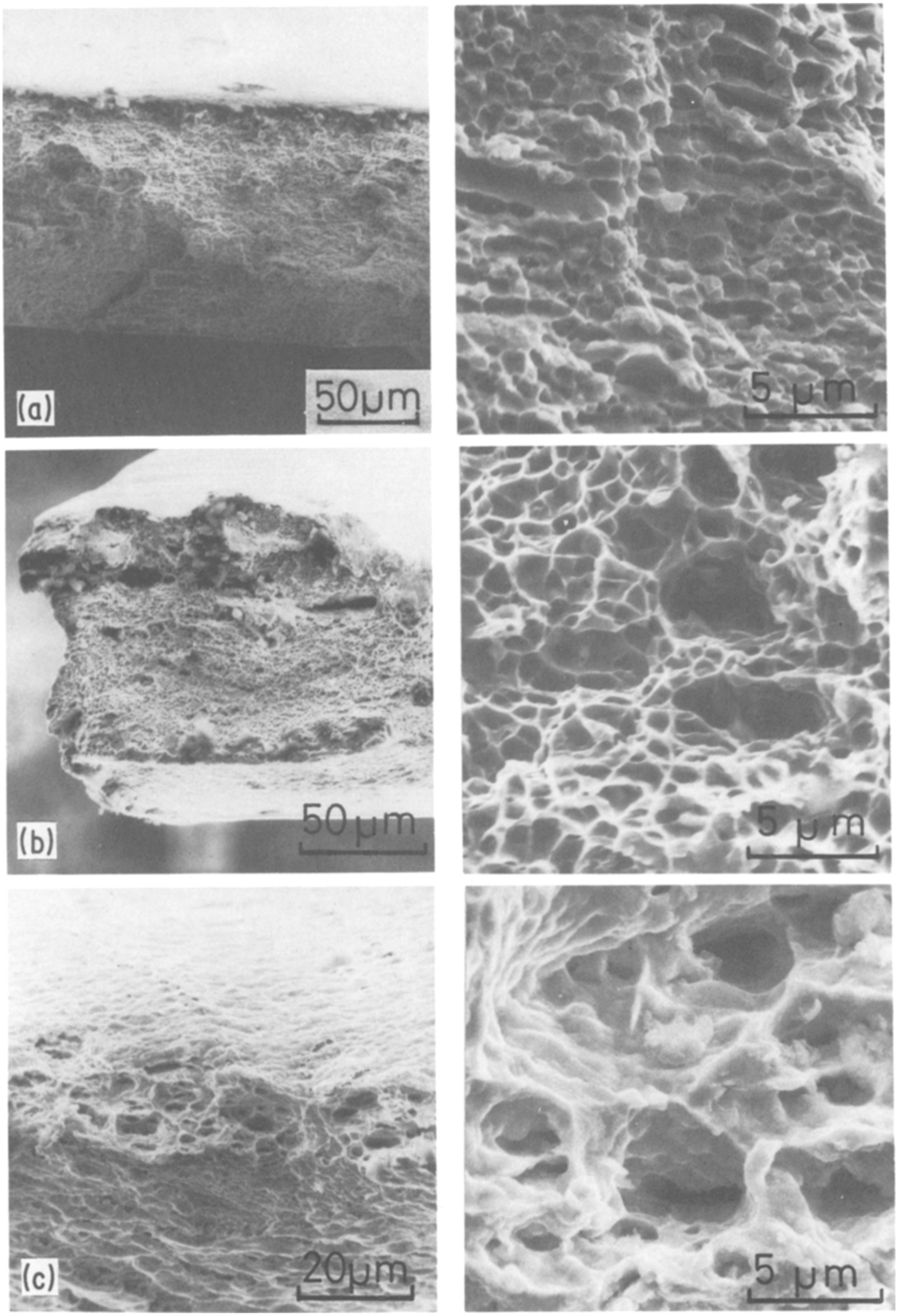

Figure 5 Fracture surfaces of Alloy 1 tested at (a) room temperature, (b) 470° C and (c) 600° C.

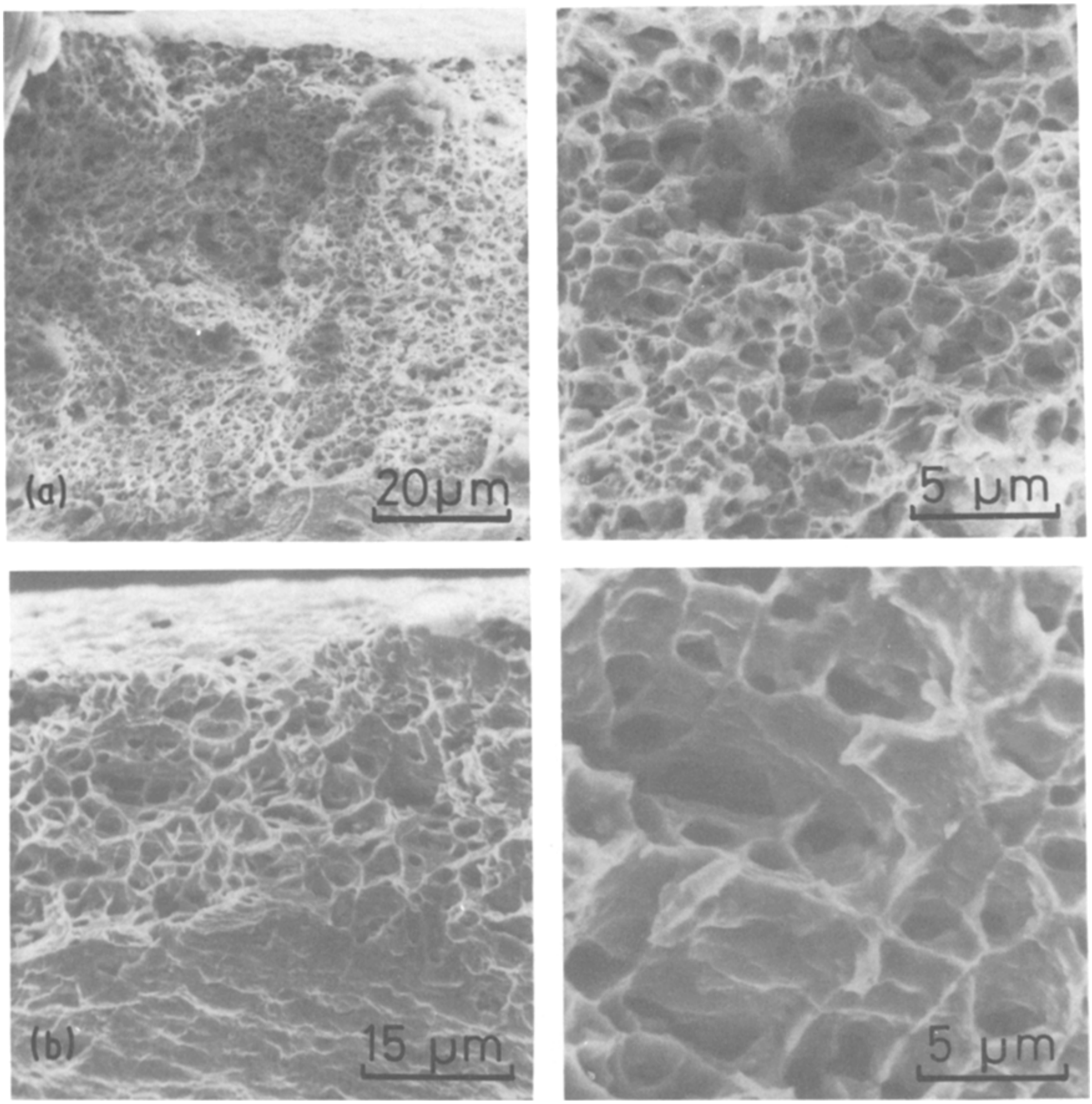

Figure 6 Fracture surfaces of Alloy 2 tested at (a) room temperature and (b) 600° C.

Fig. 6 shows that cracking starts in the relatively large χ-phase ($\geqq 1.0\,\mu$m) which cross with slip steps. However, at χ-phases smaller than $0.5\,\mu$m, cracking was not observed. The number of cracks on the free surface was larger than that in the interior. The χ-phases on the free surface crack at smaller shearing stresses than in the interior because they are less restricted by the matrix.

At the beginning of inhomogeneous deformation, which might correspond to the time of the first χ-phase cracking, the deformation band crosses the specimen in a direction perpendicular to the stress axis and the specimen fractures immediately. Thus, the first χ-phase cracking resulting in surrounding χ-phase cracking, leads to specimen fracture. Fig. 9 shows this process and it is summarized as follows:

(1) Dislocations pile up at the χ-phase on their glide plane due to matrix deformation.

(2) A χ-phase on the free surface cracks first when enough dislocations pile up at it.

(3) The two pieces of cracked χ-phase then separate due to the applied stress and a void grows in the direction parallel to the stress axis. This void growth produces stress concentration on the surrounding χ-phases. Relatively large χ-phases crack.

(4) This crack-initiation to void growth process

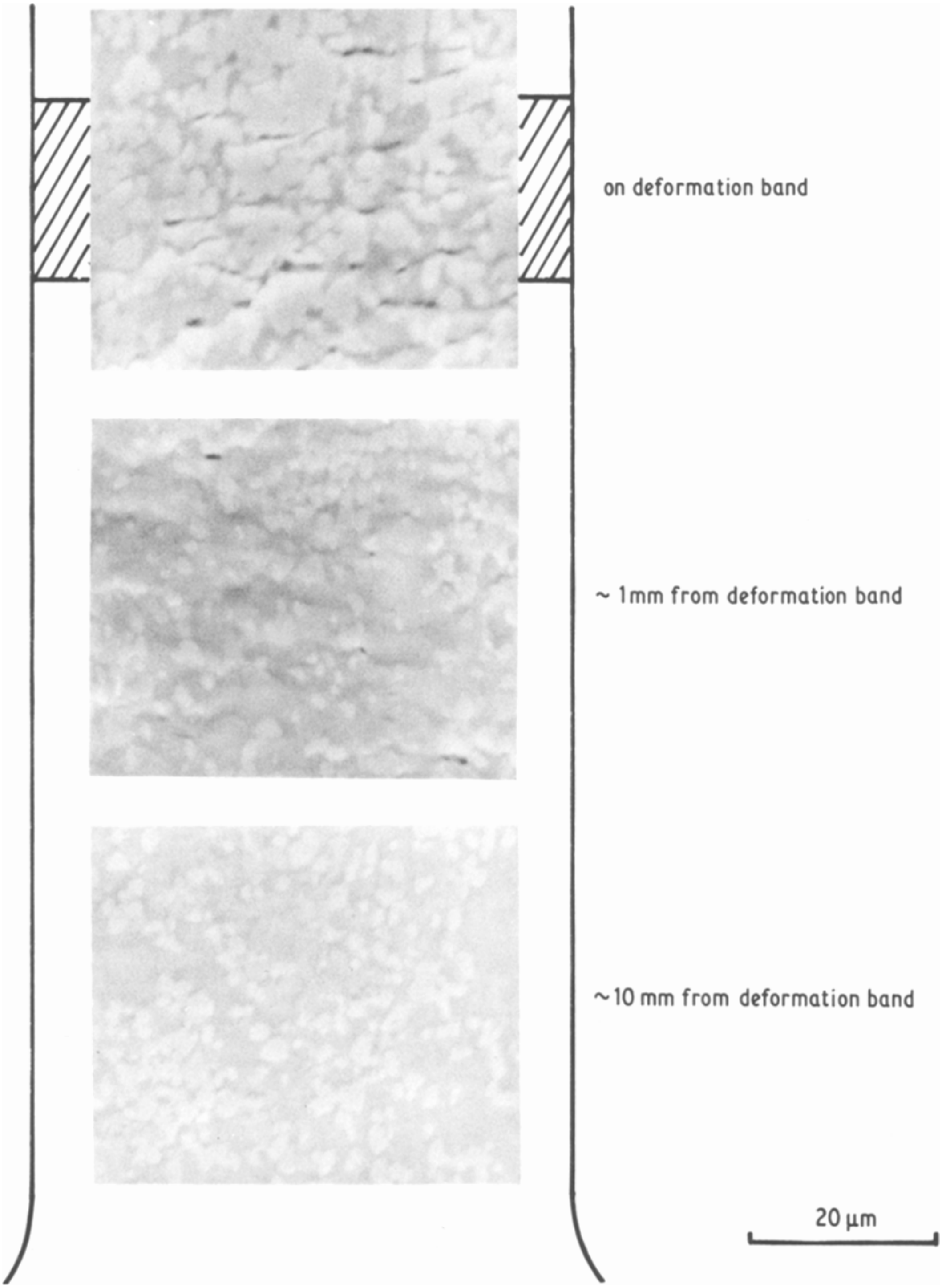

Figure 7 Crack distribution of free surface of Alloy 1 tested at room temperature just before fracture.

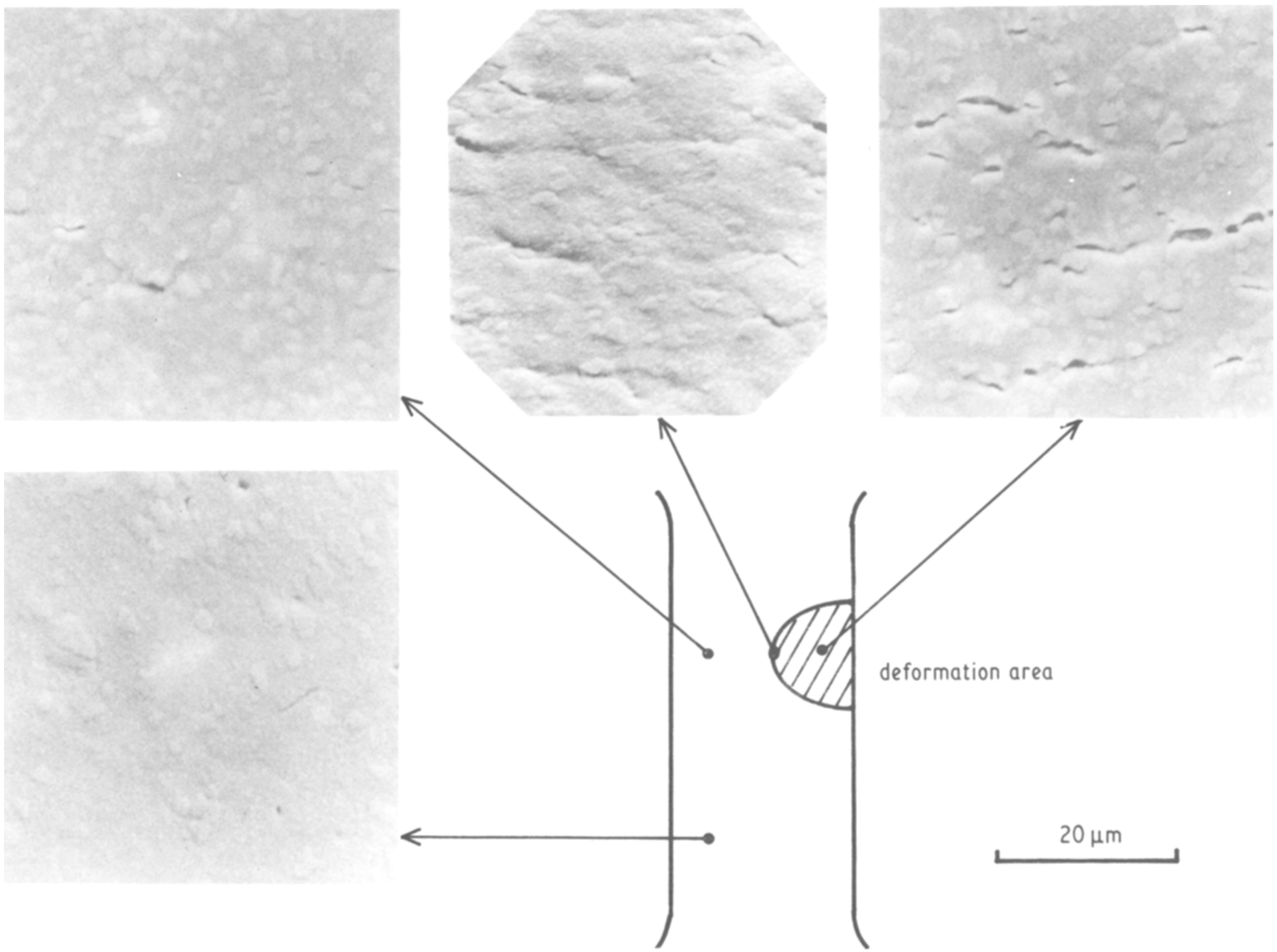

Figure 8 Crack distribution on free surface of Alloy 2 tested at room temperature just before fracture.

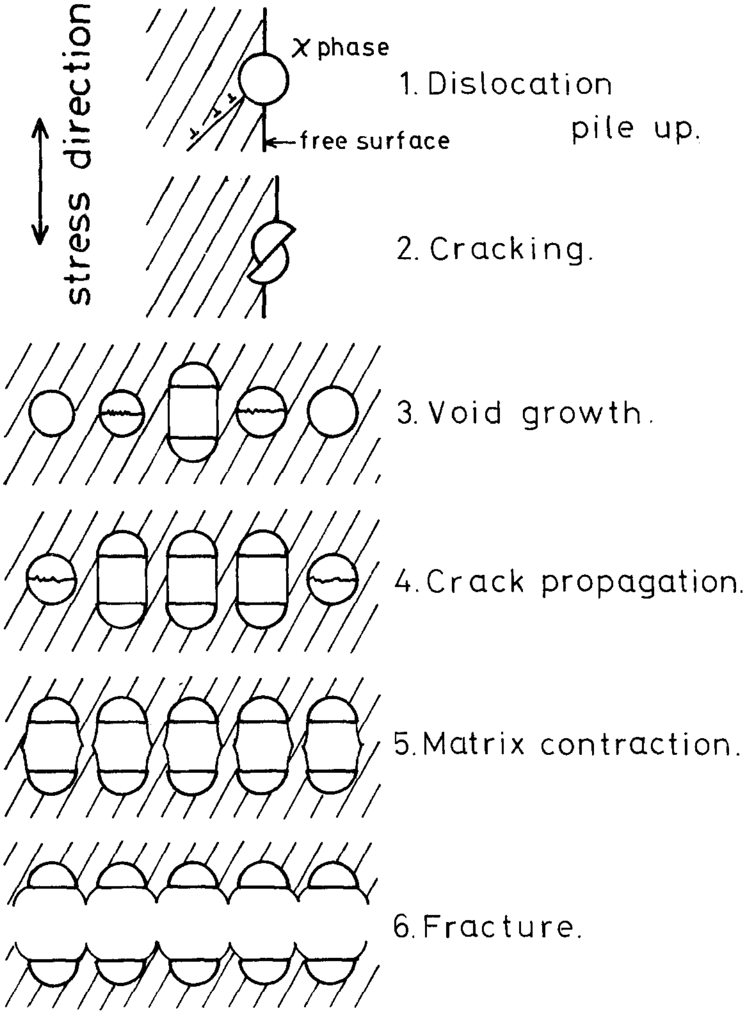

Figure 9 Schematic representation of fracture of Fe–13 wt% Cr–2 wt% Mo–2.5 wt% Ti alloy.

repeats as a chain reaction and results in the deformation band formation.

(5) After the deformation band crosses the specimen, matrix contraction occurs between voids.

(6) The specimen fracture is over when the matrix fractures.

The above mentioned mechanism indicates that each bottom of a dimple on the fracture surface will contain a faceted χ-phase and that the distribution of χ-phases will correspond to that of the dimples. This observation is plotted in Fig. 10. The broken line showss a 1-to-1 relationship and the observed points are near this line. Fig. 11 shows a typical example of a fracture surface. Thus, the fracture characteristics of this alloy are controlled by the distribution of χ-phases.

A rough estimate of the condition for one χ-phase crack to cause its neighbouring χ-phase to crack will be presented below.

In Fig. 12 when a tensile stress σ_t acts on a sharp crack of length $2C$ at χ_1, a stress σ at a distance r from the crack tip perpendicular to the tensile direction is given by

$$\sigma = \sigma_t \left(\frac{C}{2r}\right)^{1/2} \qquad (1)$$

using the elastic theory. Then the total stress acting on the χ_2 is

$$\sigma = \sigma_t \left[1 + \left(\frac{C}{2r}\right)^{1/2}\right]. \qquad (2)$$

Equation 2 indicates that if the term $(C/r)^{1/2}$ is great enough, then χ_2 can be cracked easily. Thus the term $(C/r)^{1/2}$ will be one of the ductility parameters in this alloy system. Table II shows the alloy parameter under various aging conditions. It is noticed that, although treatments 1, 3 and 4 have different χ-phase distribution characteristics

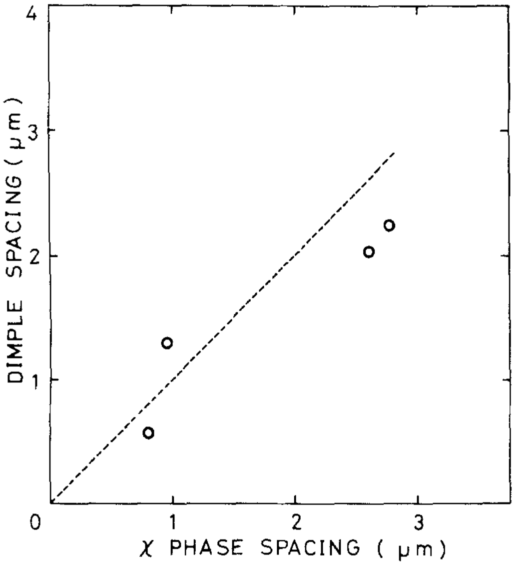

Figure 10 Relation between distributions of χ-phases and dimples. The broken lines show their 1-to-1 relationship.

$(C/r)^{1/2} \approx 0.44$ to 0.47 and that their elongation to fracture are all about 10%. Thus the term $(C/r)^{1/2}$ is a good elongation parameter of this alloy system.

4.2. Improvement of the ductility of Fe–13 wt% Cr–2 wt% Mo–2.5 wt% Ti alloy by addition of Nb

It has been proposed that 1 wt% Nb addition to Alloy 1 improved its ductility without a decrease in its strength. Intuitively one of the causes of this seems to be the decrease in the volume fraction of χ-phases larger than 1.0 μm in diameter which is the origin of brittleness in the alloy system.

In Alloy 2 χ-phase cracking was observed all over the specimen at the beginning of inhomogeneous deformation. This indicates that, before inhomogeneous deformation started, the first χ-phase cracking had already finished, which is different from the case of Alloy 1. The true stress for the first χ-phase cracking in Alloy 1 is about 91 kg mm^{-1}. At first the χ-phase cracks at the same time as in Alloy 2, corresponding to a strain of about 6.5%. If the fracture strain is considered to be about 13.0%, then Alloy 2 can be strained twice as much as in the case of the first χ-phase cracking strain. This agrees with there being no deformation band formation, which indicates that one χ-phase crack cannot cause surrounding χ-phase cracking immediately.

Figure 11 Typical example of fracture surface. Alloy 1 aged at 900° C for 8 h.

The elongation parameter $(C/r)^{1/2}$ of this alloy is about 0.58. According to Table II the fracture strain of an alloy having this value will be in the range 6.0 to 10.0%; but, in fact, it is about 13.0%. This is explained by the fine dispersion of χ-phases, less than 0.5 μm, which cannot essentially be cracked [8, 9]. Among larger χ-phases the stress concentration in front of a crack tip is relaxed.

By the above mechanism, 1 wt% Nb addition to Alloy 1 results in an improvement of ductility.

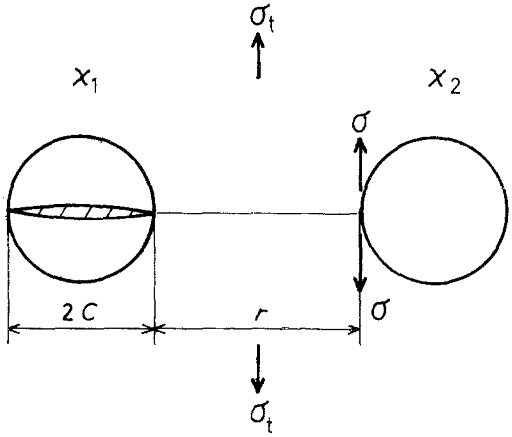

Figure 12 χ-phase cracking model.

TABLE II Alloy parameters of Alloy 1 by various aging conditions. (C is χ-phase mean radius, r is χ-phase mean spacing, ϵ is total elongation)

Treatment number	Heat treatment	C (μm)	r (μm)	$(C/r)^{1/2}$	ϵ (%)
1	700° C, 8 h	0.18	0.84	0.56	9.2
2	800° C, 8 h	0.50	1.00	0.71	6.3
3	900° C, 8 h	0.55	2.80	0.44	10.2
4	800° C, 1 h	0.16	0.70	0.47	9.6

5. Conclusion

The mechanical properties of Fe–13 wt% Cr–2 wt% Mo–2.5 wt% Ti alloy were examined by tensile tests with respect to fracture mechanism. To improve the properties, 1 wt% Nb was added and its effects were examined.

In the temperature range, room temperature to 500° C, the fracture characteristics of Fe–13 wt% Cr–2 wt% Mo–2.5 wt% Ti alloy are mainly governed by the characteristics of the χ-phase precipitation. The fracture of this alloy starts with χ-phase cracking. χ-phase cracking is propagated from the first χ-phase immediately to its surroundings and the fracture process finishes within a short period.

The term $(C/r)^{1/2}$ (C is mean χ-phase radius, r is mean χ-phase spacing) seems to be one of the good parameters for the fracture strain. The larger this term is, the smaller the fracture strain.

At high temperature, about 500° C, the χ-phase cracking ceases to occur. It seems that the fracture starts with the separation of the matrix and χ-phase at the interface.

The 1 wt% Nb addition to Fe–13 wt% Cr–2 wt% Mo–2.5 wt% Ti alloy can cause an improvement in ductility without a decrease in strength in the temperature range, room temperature to 500° C. This is explained by the fact that the term $(C/r)^{1/2}$ decreases and, in addition to this, that the fine χ-phases smaller than 0.5 μm in diameter, which seem not to crack, disperse among large χ-phases. Above 500° C, the 1 wt% Nb addition has little effect on tensile properties of this alloy.

Thus, 1 wt% Nb addition to Fe–13 wt% Cr–2 wt% Mo–2.5 wt% Ti alloy is an effective method for improving its ductility in the temperature range, room temperature to 500° C.

Acknowledgements

The authors wish to thank Professor S. Morozumi for suggestions and Mr. Narui for help with the high temperature tensile tests.

References

1. D. R. ARKELL and T. M. WILLIAMS, *J. Nucl. Mater.* **74** (1978) 144.
2. E. A. LITTLE, *ibid.* **87** (1979) 25.
3. M. SNYKERS, *ibid.* **80** (1980) 80.
4. D. KRAMER, K. R. GARR and A. G. PARD, *Trans. AIME* **245** (1969) 1909.
5. J. J. HUET and V. LEROY, *Nucl. Tech.* **24** (1974) 216.
6. H. KAYANO, K. SUGANUMA, M. NARUI, S. SUZUKI and S. YAJIMA, *J. Nucl. Mater.* **85/86** (1979) 925.
7. C. GASPARD, E. DIDERRICH, V. LEROY, J. J. HUET and L. HABRAKEN, *ibid.* **68** (1977) 104.
8. T. NAKAMURA and K. TANAKA, *Zairyo Kagaku* **5** (1968) 221.
9. A. GANGULEE and J. GURLAND, *Trans. AIME* **239** (1967) 269.

Received 14 November 1980 and accepted 29 April 1981.